Journal of Colloid and Interface Science 679 (2025) 209–220

Contents lists available at ScienceDirect

Journal of Colloid And Interface Science

journal homepage: www.elsevier.com/locate/jcis

Regular Article

Decomposition of mixed DMPC-aescin vesicles to bicelles is linked to the lipid's main phase transition: A direct evidence by using chain-deuterated lipid

Carina Dargel [a,b], Lara H. Moleiro [b,c], Aurel Radulescu [d], Tim Julian Stank [b], Thomas Hellweg [b,*]

[a] Institute of Physical Chemistry, University of Münster, Corrensstraße 28/30, Münster, 48149, Germany
[b] Physical and Biophysical Chemistry, Bielefeld University, Universitätstraße 25, Bielefeld, 33615, Germany
[c] Department of Physical Chemistry, Complutense University, Avda. Complutense s/n, Madrid, 28040, Spain
[d] Jülich Centre for Neutron Science JCNS at Heinz Maier-Leibnitz Zentrum (MLZ), Forschungszentrum Jülich GmbH, Lichtenbergstr. 1, Garching, 85747, Germany

GRAPHICAL ABSTRACT

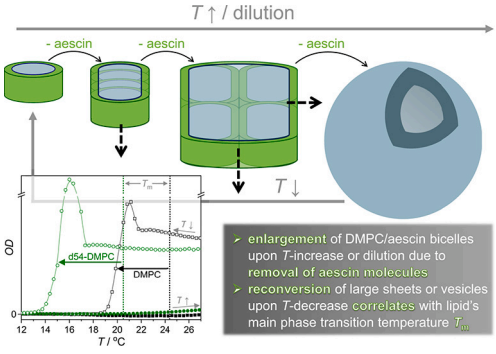

ARTICLE INFO

Keywords:
Phospholipid
1,2-dimyristoyl-sn-glycero-3-phosphocholine (DMPC)
Saponin
(β)-aescin
Scattering techniques
Bicelle-to-vesicle transition
Temperature-induced decomposition
Hysteresis
Membrane solubilization

ABSTRACT

This work investigates the conversion of bicelles into larger sheets or closed vesicles upon dilution and temperature increase for a system composed of the phospholipid 1,2-dimyristoyl-*sn*-glycero-3-phosphocholine (DMPC) and the saponin aescin. Due to its peculiar amphiphilic character, aescin is able to decompose DMPC bilayers into smaller, rim-stabilized bicelles. Aspects of the transition process are analyzed in an aescin content- and temperature-dependent manner by photon correlation spectroscopy (PCS), turbidimetry and small-angle neutron scattering (SANS). Both the conversion of bicelles into vesicles induced by temperature increase and the decomposition process upon cooling are presumably related to the main phase transition temperature T_m of DMPC. Therefore, not only conventional DMPC, but also chain-deuterated d54-DMPC was used due to its significantly lower T_m-value compared to the conventional DMPC. It will be demonstrated that the reconversion of vesicle structures (present at low aescin content) into bicelles shows a strong hysteresis effect whereas this is not observed for the reconversion at high aescin amounts, at which for high temperature still bicelle structures are present. The results indicate formation of a trapped state, correlated with the lipid's T_m and the decomposition of vesicles into bicelles is only possible if the lipid membrane entirely adopts the rigid phase state.

* Corresponding author.
E-mail address: thomas.hellweg@uni-bielefeld.de (T. Hellweg).

https://doi.org/10.1016/j.jcis.2024.10.074
Received 26 July 2024; Received in revised form 12 October 2024; Accepted 14 October 2024
Available online 18 October 2024

1. Introduction

Bicelles, sometimes also called lipid nanodiscs, are lipid-detergent aggregates which combine the monodispersity of classical micelles and the discrete bilayer-like vesicles [1]. The free-standing bilayer based on long-chain lipids (≥12 C-atoms) is rim-stabilized either by short-chain lipids or detergent molecules to protect the hydrophobic core from the hydrophilic solvent [2–4]. Among others, bicelles show the tendency to macroscopically align in an external magnetic field and are therefore used for membrane protein structure determination by NMR spectroscopy since the bicellar environment is a much more realistic membrane mimetic than detergent micelles and the proteins can adopt their native form [1,2,5,6].

In a lipid-detergent phase diagram, according to the three-stage model bicelles exist in a region between detergent micelles and lipid vesicles [7–11]: at low detergent concentration, the detergent gets incorporated into the bilayer of lipid vesicles. At some point with increasing detergent concentration, the membrane is saturated and the formation of mixed micelles begins. At very high concentration, the lipid membrane is completely solubilized and (mixed) micelles coexist with detergent monomers. The structural transition originates from the preference of the detergent to arrange in a curved manner [12,10], the different free monomer concentrations of lipids and detergents in solution and the removal of detergent molecules from the bicelles induced by dilution [10,13,14]. Moreover, a bicelle-to-vesicle transition can be achieved by temperature variation under constant lipid and surfactant concentration [15–17]. For short-chain lipids as detergents it was found that as a function of temperature increase the short-chain lipids migrate from the rim to the planar bilayer region leading to a growth of the bicelle size by coalescence effects [18]. For dilution and temperature increase a similar structural growth was observed, which in both cases is attributed to a decreased number of detergent molecules available to stabilize the bicelle rim [19].

Besides short-chain lipids also different bile salts can be used for bicelle formation in combination with phospholipids [20,21,9,14,22–25]. In comparison with short-chain lipids these molecules posses a more bulky hydrophobic portion, which is similar to the saponin used in this study. In addition, for these systems a dilution-induced transition from discoidal or rather cylindrical mixed micelles into large, elongated lamellar sheets or closed vesicles were observed. The latter can contain perforations/pores coated by detergent molecules [2,25]. Again, dilution induces the removal of bile salt molecules from the aggregated structure and exposure of the hydrophobic lipid parts to the hydrophilic solvent is compensated by a growth, resp. coalescence of the aggregates [20]. Also here, similar structural rearrangements can be induced by a temperature increase, whereby the exact structure depends on the heating rate used [22,14].

In this study, a binary system composed of the phospholipid 1,2-dimyristoyl-*sn*-glycero-3-phosphocholine (DMPC) as well as its chain-deuterated analog 1,2-dimyristoyl-*d54-sn*-glycero-3-phosphocholine (d54-DMPC) and the saponin β-aescin as a bio-surfactant are investigated. The molecular structures of all compounds are shown in Fig. 1. In general, saponins are built by either a steroidic or triterpenic hydrophobic backbone (called aglycone or sapogenin), to which in the hydrophilic glycone a varying number of sugar chains can be attached [26,27]. The saponin aescin is a natural product and can be isolated from the horse chestnut tree *Aesculus hippocastanum*. The aescin used in this study is a mixture of structurally similar molecules, whereby minor variations in the aglycone occur [28,29]. Aescin is e.g. well known as an agent for the treatment of diseases like chronic venous insufficiency (CVI) [30–32].

Due to the amphiphilic nature, aescin molecules self-assemble in solution into micelles. At room temperature, the critical micelle concentration (cmc_{aescin}) in an aqueous solution is around 0.3-0.4 mM [28]. Moreover, the amphiphilic structure of aescin enables the interaction with lipid membranes [33–36]. In earlier works, we have shown that aescin incorporates into lipid membranes composed of DMPC and modifies the bilayer parameters in a temperature- and aescin concentration-dependent manner [29,36–40]. In general, the interaction between the model membrane and aescin is stronger in the membrane's rigid state, at temperatures below the main phase transition temperature T_{m}, which is ≈ 24 °C for DMPC [29,41]. At aescin concentrations around cmc_{aescin}, the DMPC membrane is partially solubilized by the saponin and finally completely decomposed into monodisperse bicelles at $c_{\text{aescin}} \geq cmc_{\text{aescin}}$ and low temperature ($T < T_m$) [39,40]. When raising the temperature above $T_{m,DMPC}$, an increase in size leading to bigger sheets and an arrangement into stacks is shown [40]. Studies on a system composed of DMPC and the saponin glycyrrhizin showed that after temperature increase even the formation of very monodisperse, closed vesicles is possible [42].

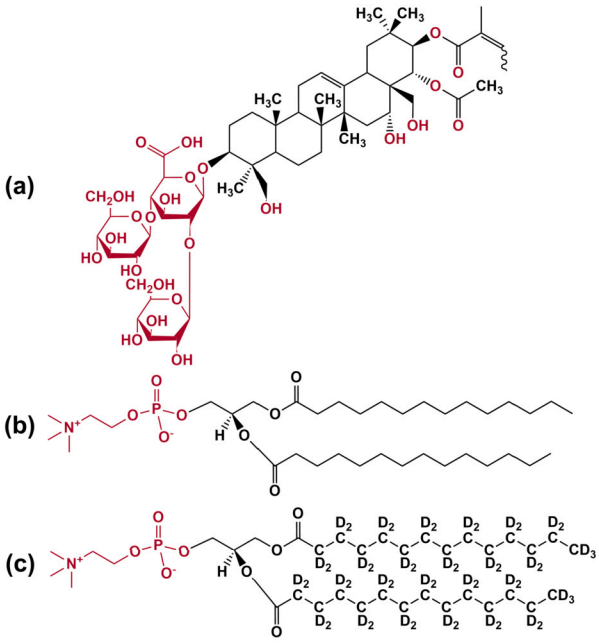

Fig. 1. Molecular structures of (a) the saponin β-aescin, (b) the phospholipid DMPC, and (c) chain-deuterated d54-DMPC. Hydrophilic molecular parts are shown in red, hydrophobic ones in black. (For interpretation of the colors in the figure(s), the reader is referred to the web version of this article.)

The present study now focuses on the process of the structural rearrangement of the DMPC-aescin system upon dilution and temperature variation. For the latter case, especially the aspect of reversibility of the transition upon heating and cooling and a possible correlation with the lipid's T_m, as known from other studies [43,18,44–46], is investigated. To directly correlate the structural and size changes with the lipid's T_m, additional to the conventional DMPC, the chain-deuterated d54-DMPC is used, which possesses a distinguishable lower $T_{\text{d54-DMPC}}$-value compared to T_{DMPC} (≈ 20.5 °C, see section 3.2), but does not modify the overall system significantly. Size changes of the self-assembled aescin-DMPC structures upon dilution will be investigated by photon correlation spectroscopy (PCS) at a constant temperature below $T_{\text{m,DMPC}}$. Size and shape changes upon temperature variation will first be followed by turbidimetry. Subsequently, these experiments are supported by small-angle neutron scattering (SANS). In both methods, conventional DMPC as well as chain-deuterated d54-DMPC will be used, but in this case not for a common contrast variation. To our knowledge, this is the first study exploiting the different T_{m} values of conventional and chain-deuterated lipids for studying the mechanism of the transition of a bicellar into a vesicular system upon temperature variation.

2. Experimental

2.1. Chemicals

The phospholipid DMPC (purity ≥ 99 %) was purchased from Lipoid GmbH (Ludwigshafen, Germany). Chain-deuterated d54-DMPC was obtained from Cortecnet (Voisins-Le-Bretonneux, France, ≥ 99 % purity, degree of deuteration = 98 %). Aescin (≥ 95 %, CAS: 6805-41-0), chloroform and deuteriumoxide (D_2O) were purchased from Sigma-Aldrich (Munich, Germany). The natural saponin used consists of cis-trans-isomers of β-aescin [28] and will conveniently be named *aescin* in this study.

All samples were prepared in a 50 mM D_2O-based phosphate buffer with a pD value of 7.4. After addition of aescin to the buffer solution, the pD-value was again adjusted to a value of 7.4. Although the pH value was measured with a H_2O-based electrode, according to a publication by Rubinson et al. [47], it was assumed that under the given conditions the measured pH value corresponds to the pD value in the solution (p$H \approx$ pD).

2.2. Sample preparation

For all samples, a lipid mass concentration of $w_{DMPC} = 10\,\mathrm{g{\cdot}L^{-1}}$ is used. The aescin mole content x_{aescin} is defined with respect to the lipid content in solution: $x_{\mathrm{aescin}} = n_{\mathrm{aescin}}/(n_{\mathrm{(d54\text{-})DMPC}} + n_{\mathrm{aescin}})$. Besides the reference systems containing only lipid, samples with x_{aescin} between 10-40 mol% were investigated in this study. We like to point out here that due to the lower w_{DMPC} used in comparison to prior studies, the phase boundaries will be shifted to higher x_{aescin}-values.

As a reference system, small unilamellar vesicles (SUVs) prepared from DMPC and d54-DMPC were used. The preparation procedure is described elsewhere [29]. A defined size distribution of the SUVs was achieved by extrusion (21 passes through membranes with a pore size of 500 Å (Whatman, Avanti Polar Lipids Inc); extruder from Avanti Polar Lipids Inc., Alabama, USA).

Aescin-containing samples were prepared using the following procedure: the required lipid amount per sample (either DMPC or d54-DMPC) was dissolved in chloroform, which was subsequently removed using a rotary evaporator, resulting in a thin and homogeneous lipid film. This film was dried over night at 60 °C to remove chloroform residues. A deuterium-based aqueous aescin buffer solution at the desired aescin concentration was added to rehydrate the lipid film and to generate mixed lipid-aescin particles.

The solutions were repeatedly frozen in liquid nitrogen and warmed up in hot water of a temperature of ≈50 °C (five repetitions). To remove bigger aggregates and dust particles all samples were filtered through a cellulose acetate filter with a pore size of 200 nm (VWR International GmbH, Darmstadt, Germany) in a cold room at a temperature well below T_m ($T < 10$ °C). Before investigation, all samples were heated and cooled several times between 10 and 60 °C to ensure the formation of equilibrium structures.

2.3. Photon correlation spectroscopy (PCS)

Photon correlation spectroscopy was used to determine the size of the mixed lipid-aescin particles in solution in terms of the hydrodynamic radius R_{H}. The theoretical background for the determination of R_{H} can be found in the Supplementary Material.

PCS measurements were performed in NMR tubes on a 3D light scattering goniometer setup (LS Instruments AG, Fribourg, Switzerland) equipped with a HeNe laser with $\lambda = 632.8$ nm (JDSU 1145P, Milpitas, California, USA) in modulated 3D correlation mode. The autocorrelation function was generated with a multiple-τ-digital correlator (correlator.com, USA) and recorded at scattering angles between 40 ° and 110 ° in steps of 5 ° at a temperature of 12 °C. Before filling the samples into NMR tubes the samples were centrifuged at 10000 rpm for 20 min. The data obtained was analyzed using the CONTIN program [48]. Here, not only samples with a DMPC mass concentration of $10\,\mathrm{g{\cdot}L^{-1}}$ were used. The samples were diluted with buffer solution to lower DMPC mass concentrations down to $0.5\,\mathrm{g{\cdot}L^{-1}}$.

2.4. Turbidimetry

Turbidimetry was used to estimate the temperature-dependent size evolution of the investigated samples. The measured attenuation of light intensity, convertible into the optical density OD, is mainly dependent on the particle size and the particle concentration in solution. OD is the sum of absorption and scattering of light by particles, but absorption processes can be neglected by choosing an adequate wavelength at which none of the substances is absorbing. Therefore, the detected OD is approximately proportional to the particle size [49].

Turbidimetry measurements were performed on an Agilent 8453 UV-visible spectrometer (Agilent Technologies, Santa Clara, USA). The spectrometer is equipped with a 8-position sample holder and the temperature is externally controlled with a thermostat. The samples were measured in screw cap quartz cuvettes with a path length of 2 mm (Starna Scientific GmbH, Pfungstadt, Germany) to avoid solvent evaporation. All samples were measured at the same sample position and the temperature was recorded with a PT-104A resistance thermocouple (Omega, Deckenpfronn, Germany) in the reference cuvette which was filled with buffer solution. Data were recorded in a wavelength range of 200-800 nm and final evaluation was done at a wavelength of 400 nm. All measurements were performed in an effective temperature range of ≈10-70 °C with a heating/cooling rate of $k \approx 40$ °C/h. To ensure the reversibility of the structural transition, four consecutive heating/cooling cycles were performed. The system was equilibrated at the highest and lowest temperature for one hour after each heating/cooling step.

2.5. Small-angle neutron scattering (SANS)

In this study, the small-angle neutron scattering technique (SANS) is used to determine the structure and temperature-dependent structural changes of mixed lipid-aescin particles with different x_{aescin}. A description of the theoretical background can also be found in the Supplementary Material.

Briefly, SANS was used because the particle under investigation possesses a high contrast to the deuterated solvent used. In addition, chain-deuterated d54-DMPC was investigated to examine the particles with an internal membrane contrast. In general, two different techniques were used to determine particle size and shape. The pair distance distribution function $\rho(r)$ and the radius of gyration R_G of the particles were determined from the model-independent Indirect Fourier Transformation (IFT) method [50–52]. In addition, the scattering data were fitted using specific models to obtain detailed information about the particles shape. Descriptions of the individual models as well as the assumptions regarding sizes of the molecules and associated scattering length densities (SLDs) are presented in detail in the Supplementary Material. The program SASView was used for fitting [53].

SANS experiments were performed at the KWS-2 instrument at the Heinz-Meier Leibnitz Zentrum (MLZ) in Garching (Munich, Germany) [54]. The samples were filled into 2 mm screw cap quartz cuvettes (Starna Scientific GmbH, Pfungstadt, Germany) and measured in a 8-position thermostated Peltier sample holder. First, the samples were heated step-wise from 10 °C to 60 °C and cooled (again step-wise) to 10 °C afterwards. Between two temperatures fast heating/cooling rates of ≈ 20 °C/min were used. The equilibration time at each temperature was 20 min. A q-range from $2{\cdot}10^{-3}$ Å^{-1} to 0.4 Å^{-1} was covered using a neutron wavelength of 5 Å at sample-to-detector distances of 2 m, 8 m, and a neutron wavelength of 10 Å at 20 m. The wavelength resolution was $\Delta\lambda/\lambda = 10$ %. Initial treatment of the 2D data was performed with the software QtiKWS [55]. Absolute scale was obtained by using plexiglass as standard.

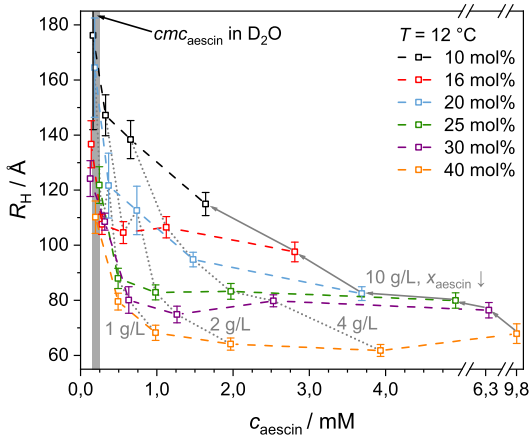

Fig. 2. R_H as function of c_{aescin} in the samples with different x_{aescin} and different w_{DMPC}. Lines in the color of the data points link samples with the same x_{aescin}, whereas grey lines link samples with the same w_{DMPC}. R_H increases with decreasing aescin content x_{aescin}, especially in the region of the cmc_{aescin} (highlighted in grey).

3. Results and discussion

Previous studies on mixed DMPC-aescin aggregates have shown that the size of the bicelles, which are formed at temperatures well below the lipid's T_m and from aescin concentrations around cmc_{aescin} (corresponding to 6-7 mol% at a lipid mass concentration of 15 mg·mL^{-1}) depends on the ratio of the lipids and the aescin molecules [38–40]. In this study, special attention was paid to the completely reversible structural changes of the DMPC-aescin mixtures as a function of temperature and its correlation with the lipid's T_m. First, the effect of dilution on the bicelle size is evaluated.

3.1. Size increase of DMPC-aescin particles upon dilution as seen by PCS

The PCS method was exploited to determine the bicelle size at a defined temperature well below $T_{m,DMPC}$ as function of both the DMPC mass concentration w_{DMPC} and the aescin content x_{aescin}. Therefore, the hydrodynamic radius R_H for samples containing between 10 and 40 mol% aescin at initial w_{DMPC} of 10 g/L was determined. Moreover, the samples were diluted to lower w_{DMPC} (down to 0.5 g/L) which changes the lipid-aescin ratio in each bicelle as well as the absolute aescin concentration c_{aescin}. This is expected to result in a size increase of the bicelles with a decrease of both w_{DMPC}, and x_{aescin}.

The hydrodynamic radius R_H can be represented as a function of various parameters. Fig. S1 in the Supplementary Material shows R_H as a function of the DMPC mass concentration w_{DMPC} (at different x_{aescin}, see Fig. S1a)), as well as as a function of x_{aescin} (for different w_{DMPC}, see Fig. S1b)). Since a correlation of R_H with the absolute aescin concentration in the sample (c_{aescin}) is to be established, a direct representation of the dependence of R_H and c_{aescin} is also possible. This is shown in Fig. 2. To connect the change in R_H with the critical micelle concentration of aescin (cmc_{aescin}), in all figures cmc_{aescin} is indicated by a grey area/line. cmc_{aescin} in D_2O-based phosphate buffer was determined by measurement of the surface tension of aescin solutions at a temperature of 12 °C (see Fig. S2). Table S1 additionally lists all parameters, w_{DMPC}, x_{aescin}, c_{aescin} and R_H and additionally the polydispersity index PDI_{R_H} of each sample. The dependencies shown in Fig. S1 can also be read from Fig. 2: data points with the same color mark samples with the same x_{aescin}. Additionally, data points connected with a grey line denote samples with different x_{aescin} but constant w_{DMPC}.

From the dependence of R_H and x_{aescin} (see Fig. S1a)), it can be concluded that a reduction of x_{aescin} results in an increase in bicelle size. This was also already found in an earlier work [40]. The number of aescin molecules per DMPC molecule (A/D) in each bicelle is reduced and therefore, fewer aescin molecules are available to form the bicelle belt, which is why there are fewer, but larger bicelles overall. The plot of R_H as a function of w_{DMPC} for different x_{aescin} (see Fig. S1b)) now additionally shows that a significant size increase, independent of x_{aescin}, only occurs at $c_{aescin} \approx cmc_{aescin}$ or below. From this, it can be concluded that at $c > cmc_{aescin}$ there are enough aescin molecules available to form bicelles. This is a clear indication that only *excess aescin* is available for the formation of bicelles; a basal concentration of aescin always remains in solution (theoretically present in the form of monomers in solution in the concentration of approx. cmc_{aescin}). When diluting the entire sample, and thus reducing w_{DMPC} and c_{aescin}, the number of excess aescin molecules available for bicelle formation is also reduced, which leads to an increase in the bicelle size. Formation of bare bicelles with monodisperse and narrow size distribution seems only to be possible at $c_{aescin} > cmc_{aescin}$, which is supported by the high polydispersities PDI_{R_H} which were found at aescin concentrations around cmc_{aescin}.

In the following, structural size and shape changes upon heating and cooling will be investigated in comparison to the observed dilution effect. Only the samples with the initial w_{DMPC} of 10 g·L^{-1} were investigated, because these samples show structures with a very low polydispersity of only 7-11 % and are most suitable for SANS measurements due to the comparably high w_{DMPC}. It is expected that structural changes upon heating/cooling accompanied with a change of the phase state of the continuous DMPC bilayer also modify the DMPC-aescin ratio in the bicelles due to solubility effects.

3.2. Turbidimetry measurements reveal hysteresis of the structural rearrangement upon cooling

Turbidimetry can be used to estimate the size changes of the DMPC-aescin particles, e.g. as a function of temperature, because the detected optical density OD roughly correlates with the particle size [49]. Here, this method is used while continuously and repeatedly heating and cooling the samples and correlating the temperature-dependent OD evolution with the T_m of the lipid used. To establish a direct correlation with T_m, additional to the conventional DMPC the chain-deuterated analog d54-DMPC was used. The specific T_m-values of both lipids were extracted from the temperature-dependent turbidity change of DMPC as well as d54-DMPC SUVs (see Fig. S3). Therefore, the OD is converted into a degree of conversion and the derivative thereof yields both T_m values. Since $T_{m,d54\text{-}DMPC}$ is about 4 °C lower compared to $T_{m,DMPC}$, T_m-correlated structural changes of the DMPC-/d54-DMPC-aescin systems can clearly be distinguished.

Only samples with $w_{(d54\text{-})DMPC} = 10\,g{\cdot}L^{-1}$ were investigated to directly compare the results obtained from turbidimetry with results from neutron scattering later on. Three representative samples were chosen: one with $c_{aescin} \approx cmc_{aescin}$ (10 mol% aescin), one with $c_{aescin} \gg cmc_{aescin}$ (30 mol% aescin) and one sample in between still showing pronounced structural changes (16 mol% aescin). All samples were repeatedly measured in a temperature range between 10 and ≈70 °C and changes in OD are viewed at a wavelength of 400 nm. At this wavelength, none of the substances shows absorption (see Fig. S4). Therefore, OD-changes can directly be correlated with structure-related size changes of the lipid-aescin particles.

Fig. 3 shows the continuous $OD(T)$-profiles for all x_{aescin} and both lipids, DMPC and d54-DMPC with the T_m values indicated each. The data correspond to one consecutive heating and cooling cycle. For the samples containing 30 mol% aescin a temperature dependence of the OD cannot be observed for both lipids. Due to the very high aescin-DMPC ratio, increasing the temperature — and thereby potentially reducing A/D because of the increased solubility of aescin in the aqueous solution — might lead to a size change, which, however, is not detectable by turbidimetry. This is supported by the results of a recent NMR study performed on exactly this system [56]. It was shown that a reversible temperature-dependent progression takes place which mainly involves

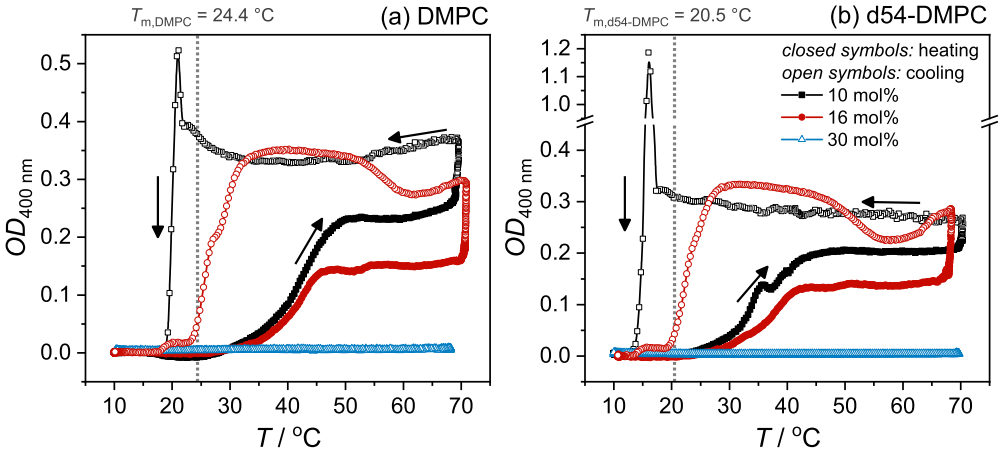

Fig. 3. OD in dependence on the temperature for samples with (a) DMPC and (b) d54-DMPC with aescin contents of 10, 16 and 30 mol% aescin. The samples were heated and cooled with a heating/cooling rate of ≈ 40 °C/min. For samples with lower aescin contents (10 and 16 mol% aescin) a reconversion around the lipid's T_m can be observed, as indicated by the vertical grey line. The sample with 30 mol% does not show a temperature dependence detectable by turbidimetry.

fast processes such as rearrangements of the rim and/or dissolved aescin molecules taking place within individual bicelles. Here, the removal of aescin molecules from the particles was not a dominant factor. For the samples containing 10 and 16 mol% aescin, upon temperature increase a similar behavior is observed: well above T_m of the lipid, the OD increases until it reaches a plateau. At highest temperature (≈ 70 °C) the samples were equilibrated for one hour and the OD increases although a plateau was reached before and the temperature is kept constant. Such an increase was observed reproducibly. However, a structural rearrangement during equilibration could not be confirmed by subsequent SANS measurements so that only assumptions could be made about the background process underlying this observation.

When decreasing T, the samples with 10 and 16 mol% each show a characteristic decline to the original, very low OD. For the sample with 16 mol% aescin, a three-step-like reconversion process was observed for both lipids (DMPC and d54-DMPC), whereby the first step occurs above T_m, the second at ≈ T_m and the last well below T_m of the lipid. Since the behavior is very similar for both lipids, a coherence of the reconversion process with the lipid's T_m is indicated. For the sample containing 10 mol% aescin, the decline to low OD occurs in one very steep step taking place ≈5 °C below the lipid's T_m, again very clearly indicating a correlation with the lipid's T_m. For this sample it looks like it is approaching a *trapped state* with decreasing temperature, which spontaneously decomposes back to small bicelles when the lipid is present solely in the solid/crystalline state. Formation of a *trapped state* is again supported by the results of the NMR study [56]. Close inspection shows that also for the sample with 16 mol% aescin this is the final step of the reconversion process. In Fig. S5, the $OD(T)$-profiles for the samples containing 10 and 16 mol% aescin are again compared, showing the very similar general OD-trace and moreover highlighting the shift in temperature especially for the cooling period. This shows on the one hand that the general behavior of the system is not significantly influenced by the deuteration of the lipid. On the other hand, the structural rearrangement, especially during cooling, seems to be related to the lipid's T_m since the reduction of the OD to the initial value takes place in a very narrow temperature range with an equal offset relative to T_m ((4.3 ± 0.2) °C for DMPC and (5.0 ± 0.3) °C for d54-DMPC). All measurements were performed at a constant heating/cooling rate. We would like to point out that the general temperature-dependent process is independent of the cooling rate used in this experiment. However, a slight shift in the effective transition temperature may occur depending on the heating/cooling rate, which can be explained by the different time periods for the system to respond to the temperature changes (see Fig. S6).

3.3. Small-angle neutron scattering (SANS): structures involved in the temperature-dependent rearrangement process

3.3.1. Model description and characterization of the (d54-)DMPC-reference system

To quantify the structures underlying the transitions observed by turbidimetry and to correlate these with the $OD(T)$-behavior as well as the correlation of the reconversion process with the lipid's T_m, SANS experiments were performed on samples with $w_{(d54\text{-})DMPC} = 10\ g{\cdot}L^{-1}$ and aescin amounts of 10, 16 and 30 mol% in a temperature range between 10 and 60 °C in steps of 5 °C. A fast heating rate between two different temperatures (at least 20 °C/min) was chosen to become independent of aggregation effects on the membrane scale. To illustrate such heating rate-dependent effects additional small-angle X-ray scattering (SAXS) experiments were performed. The respective results are shown in the Supplementary Material (among others in Fig. S7).

Previous investigations on the aescin-DMPC system showed that at $c_{aescin} > cmc_{aescin}$ and $T \ll T_m$, the continuous DMPC bilayer is entirely solubilized by the aescin molecules into mixed bicelles. Upon increasing the temperature, these bicelles combine to form larger sheet structures, with their rims stabilized by aescin molecules. [39,40]. Also formation of mixed DMPC-aescin vesicles seemed possible at elevated temperatures. For that reason, three different models were used to describe the SANS data obtained from the mixed aescin-DMPC system and to derive size information about the underlying structures: the core-shell bicelle model (CSB) to describe the bicellar structures (Fig. 4(a)), the core-shell parallelepiped model (CSPE) to describe the sheet structures (Fig. 4(b)), and the core multi shell sphere model with three shells (CMS) to describe the SUV structures (Fig. 4(c)). The last model is also used to describe the reference SUVs composed of only (d54-)DMPC. All models are provided by the small-angle scattering analysis software package SASView [53] and descriptions concerning the size and contrast parameters, the latter expressed by the neutron scattering length density $NSLD$ contained in the respective models, and assumptions made during fitting can be found in the Supplementary Material (e.g. in Table S2).

Here, first the SUV reference systems fabricated of each lipid, DMPC and d54-DMPC, are considered with the final aim to determine the T_m value for each lipid system to relate these values to the structural transitions in the mixed DMPC-aescin system. For this, the SANS signals of the DMPC- and d54-DMPC SUVs were recorded in a temperature range between 10 and 60 °C (see Fig. S8) and fitted by the CMS model. Thereby, the fitting procedure was based on previous work [57,58,42]. The fit parameters are summarized in Table S3. Due to the different contrast of H- and D-atoms, the data of d54-DMPC-SUVs show a significant intramembrane head-tail contrast whereas this is absent for the DMPC-SUVs.

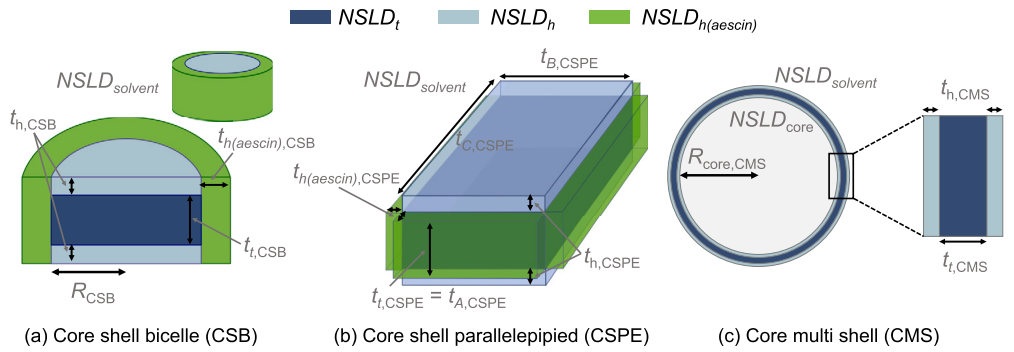

Fig. 4. Schemes for (a) the core-shell bicelle (CSB), (b) the core-shell parallelepiped (CSPE) model and (c) the core multi shell (CMS) model to describe SUVs. All models are implemented in SASView [53].

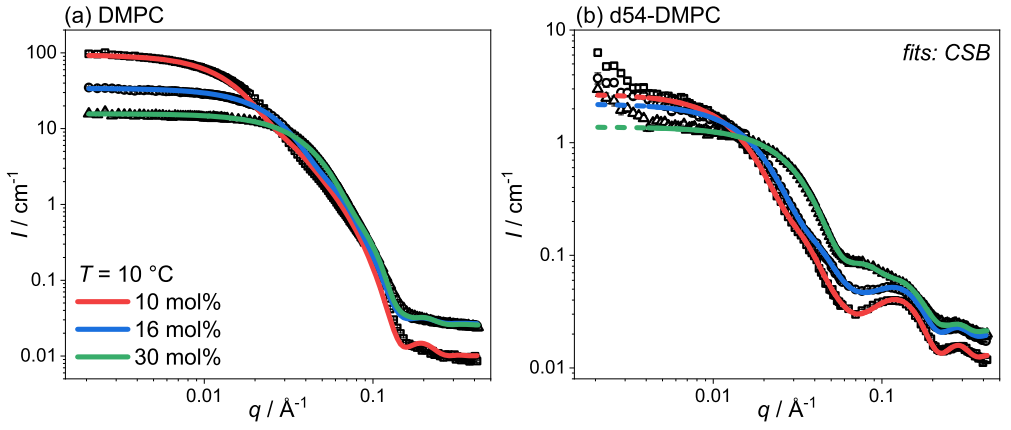

Fig. 5. SANS curves of (a) DMPC and (b) d54-DMPC containing different amounts of aescin at a temperature of 10 °C. Solid lines are fits with the CSB model from SASView [53]. The fit parameters are summarized in Table 1.

$NSLD$-profiles of the (d54-)DMPC-membrane were derived from CMS-fitting and are shown as a function of the distance from the middle of the bilayer in Fig. S9.

The CMS-fit yields the core radius $R_{core,CMS}$, its polydispersity $\sigma(R_{core,CMS})$ and the thickness of the lipid's tail part $t_{t,CMS}$ which is convertible into the total membrane thickness $t_{M,CMS}$. For d54-DMPC, moreover the polydispersity of the tail thickness $\sigma(t_{t,CMS})$ was determined. The mentioned as well as further fit parameters such as $NSLD$ values are summarized in Table S3. In Fig. S10, $t_{M,CMS}$ is plotted as a function of temperature T and from a sigmoidal fit the T_m-values for both lipids were determined. In concordance with previous turbidimetry measurements, $T_{m,d54\text{-}DMPC} = 20.1 \pm 1.1$ °C is significantly lower than $T_{m,d54\text{-}DMPC} = 25.8 \pm 0.9$ °C.

3.3.2. Characterization of DMPC-aescin bicelles at $T < T_m$

The mixed DMPC-aescin system was also measured in a temperature-dependent manner to follow the structural changes upon heating and cooling, and to correlate these changes to the lipid's T_m. Here, first the particles present at $T < T_m$ were focused. The SANS data for both lipids and all x_{aescin} are displayed in Fig. 5(a) for conventional DMPC and (b) for chain-deuterated d54-DMPC. Again, the effect of chain deuteration becomes visible in the pronounced scattering contribution of the phospholipid bilayer at high q around ≈ 0.15 Å^{-1}. Prior PCS measurements showed the presence of very small and monodisperse particles (compare Fig. 2 and Table S1) which correspond to mixed bicelle structures. To gain precise information about the bicelle size parameters the data were fitted with the CSB-model (see solid lines in Fig. 5), which is similar to a model used in previous work to describe these structures [39,40]. The CSB fit parameters, namely the bicelle radius R_{CSB} with its polydispersity $\sigma(R_{CSB})$, the thickness of the inner tail part $t_{t,CSB}$ and hence the total membrane thickness $t_{M,CSB}$ as well as the thickness of the aescins head group $t_{h(aescin),CSB}$, are summarized in Table 1, corresponding $NSLD$ values are shown in Table S4. For all samples a good agreement of the experimental data and the CSB model is found. For both lipids, the results again confirm that higher amounts of aescin lead to smaller bicelles, which is in agreement with earlier work [39]. In general, the very similar results for both lipids indicate that the overall system is not significantly modified by the partial deuteration of the lipid.

In the fit procedure, the thickness of the aescin head groups $t_{h(aescin),CSB}$ was not fixed. The aim was to use the results as reasonable values for further evaluation. $t_{h(aescin),CSB}$ increases with increasing x_{aescin} and the obtained values of ≈14 Å are in the same range as the value obtained by Penfold et al. [59]. The increase of $t_{h(aescin),CSB}$ might result from the decrease of the bicelle size with increasing x_{aescin} and therewith an increasing angle between neighboring aescin molecules. The penetration of the aescin molecules into the lipid bilayer might therefore be hindered at high x_{aescin}. Based on the results obtained, $t_{h(aescin),CSB}$ is fixed to a value of 14 Å in the further fitting procedure. The scattering data of d54-DMPC shows an upturn at low scattering angles, which might arise from weak aggregation effects. These effects do not influence the whole temperature-dependent transition process significantly (see comparison for DMPC and d54-DMPC in Fig. 3).

3.3.3. Characterization of DMPC-aescin structures after increase of T above T_m

To investigate the structural change after T-increase (especially above T_m), scattering curves of all aescin containing samples as well as the reference SUVs for both lipids are shown for a temperature of 35 °C in Fig. 6. The main structural rearrangement occurs around and slightly above the lipid's T_m (compare Fig. 3) and scattering curves at 35 °C are representative for all temperatures well above T_m (compare Fig. S11-S17 showing the full data sets). The data in Fig. 6 are fitted by

Table 1
Summary of fit parameters obtained from CSB model to scattering data at 10 °C. The parameters are the bicelle radius R_{CSB} and its polydispersity $\sigma(R_{CSB})$, the thickness of the inner tail parts $t_{t,CSB}$, the total membrane thickness $t_{M,CSB}$, the thickness of the DMPC head group $t_{h,CSB}$ (fixed to a constant value), and the thickness of the aescins head group $t_{h(aescin),CSB}$. Corresponding $NSLD$ values can be found in Table S4.

x_{aescin} / mol%	DMPC			d54-DMPC		
	10	16	30	10	16	30
R_{CSB} / Å	141.7±0.5	76.5±0.2	44.6 ±0.2	114.7±2.3	84.4±1.5	38.9±0.5
$\sigma(R_{CSB})$ / %	15.3±0.4	10.5±0.4	9.1±0.4	20.8±0.7	24.6±0.6	27.3±0.7
$t_{t,CSB}$ / Å	29.3±0.1	28.7±0.1	27.7±0.2	33.2±0.3	33.3±0.3	33.5±0.4
$t_{M,CSB}$ / Å	47.3±0.1	46.7±0.1	45.7±0.2	51.2±0.3	51.3±0.3	51.5±0.4
$t_{h,CSB}$ / Å	9.0±0.1	9.0±0.1	9.0±0.1	9.0±0.1	9.0±0.1	9.0±0.1
$t_{h(aescin),CSB}$ / Å	10.2±0.6	13.4±0.3	13.7±0.1	10.5±0.4	12.0±0.4	15.3±0.3

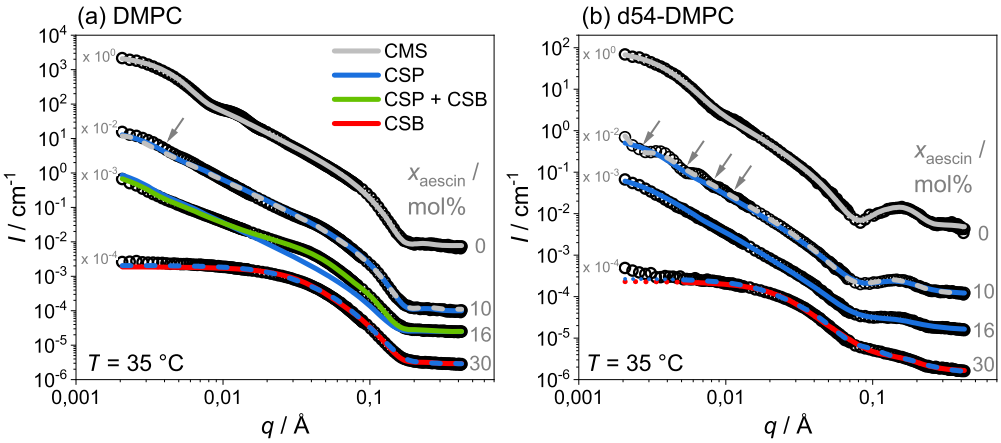

Fig. 6. SANS curves of (a) DMPC and (b) d54-DMPC containing different amounts of aescin at a temperature of 35 °C. The scattering data was approximated by the CMS, CSPE and CSB models from SASView [53,60]. Fit parameters for all models are given in Table S5/S6. Grey arrows mark form factor minima of the sample containing 10 mol% aescin.

the models presented in Fig. 4 and all fit parameters are summarized in Table S5 for DMPC and Table S6 for d54-DMPC. As already shown, the reference system could be nicely fitted by the CMS model irrespective of T and yielded SUV particles with a core radius of $R_{core,CMS} \approx 250$ Å, but with a high polydispersity resulting from the preparation procedure. Fig. 6 now reveals the shapes of the aescin-containing samples present at $T > T_m$.

The samples with the highest x_{aescin} investigated (30 mol%) underwent a rather small structural change, as the SANS data is still similar to the data obtained at 10 °C (see Fig. 5). This is in line with results from turbidimetry as well as NMR from a preceding study [56]. The data is still representable by the CSB model but the particles do not strictly have to possess a spherical base shape anymore, which is why the CSPE model was applied as an alternative model. This model was previously used to describe elongated DMPC-aescin particles [40]. It describes the hydrophobic part of a DMPC membrane that is spanned by a rectangle with side lengths $t_{B,CSPE}$ and $t_{C,CSPE}$ (compare Fig. 4(b)). The height corresponds to two times the lipid chain length and is described by $t_{A,CSPE} = t_{t,CSPE}$. The lipid head groups are additionally considered by $t_{h,CSPE}$. The entire lipid membrane is from the outside surrounded by an aescin belt, which is characterized by the thickness $t_{h(aescin),CSPE}$. The agreement of the data with the CSPE fit was indeed slightly better compared to the CSB model and the sheet areas obtained from fitting clearly indicate that the particles elongate in a preferred direction, maybe due to migration of aescin molecules from the rim into the bilayer. The sheet area of the DMPC-based systems is ≈ 64x177 Å^2 (≈ 11300 Å^2) and a value of ≈ 62x235 Å^2 (≈ 14600 Å^2) was obtained for the d54-DMPC-based system. In comparison with the bicelle size of these samples at 10 °C ($R_{CSB(DMPC)} \approx 45$ Å (ground area ≈ 6400 Å^2) and $R_{CSB(d54\text{-}DMPC)} \approx 39$ Å (ground area ≈ 4800 Å^2)) the aggregates increased their size by a factor of 2-3. In SANS, this size change is clearly detectable, whereas turbidimetry is not sensitive enough to detect this size change.

It is expected that also the samples with $x_{aescin} = 10$ and 16 mol% can be represented by the CSPE model at $T > T_m$. Due to the lower A/D-ratio in the bicelles and the overall lower c_{aescin}, the formation of much larger sheets is expected due to fusion of several bicelles, induced by a slow removal process of aescin molecules from the bicelle rim [56]. Hence, first the sample with $x_{aescin} = 16$ mol% was approximated by the CSPE model (see Fig. 6(a) for DMPC and (b) for d54-DMPC). In the case of d54-DMPC, the agreement of the model fit with the scattering data is good and a highly asymmetric sheet with an area of ≈950x1850 Å^2 is determined. For conventional DMPC a deviation of the experimental data from the CSPE fit is observed and in this case a combination of the CSPE and CSB model is necessary to fit the data adequately. The share of bicellar structures is still ≈ 66 %. Such a behavior was not expected, but literature reported that a coexistence of more than one shape of aggregate is possible [12]. Inhomogeneities in the sample might have caused that not all structures have undergone the same transition. The CSPE share of the fit showed an area of ≈1650x1864 Å^2, which is less asymmetric compared the d54-DMPC system. Here, it has to be kept in mind that the results are most probably influenced by the high share of bicelles present.

The scattering data of the sample containing 10 mol% aescin can as well be approximated by the CSPE model, but the appearance of a form factor minimum at low q (in the case of the deuterated lipid even several oscillations were observed) indicates the presence of (monodisperse) SUV structures. A closure to SUVs was also described in literature [61,62,42]. For this reason, here also the CMS model was applied. CSPE fits yield lamellar sheets with an area of ≈1300x1500 Å^2 for DMPC

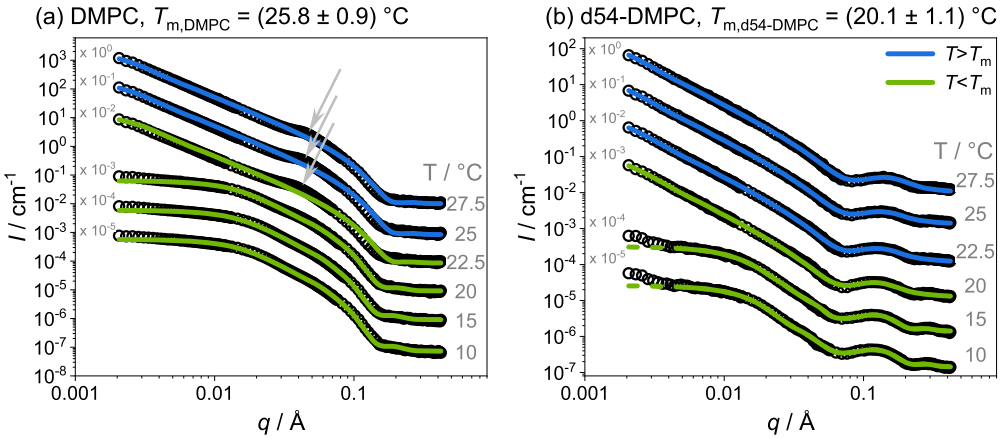

Fig. 7. SANS curves of (a) DMPC and (b) d54-DMPC containing an aescin amount x_{aescin} of 10 mol%. Data are shown for several temperatures around the lipid's T_m while cooling the samples step-wise. Solid lines are fits with the CSPE model from SASView [60,53]. All fit parameters are summarized in Table S7.

and ≈1100x1300 Å^2 for d54-DMPC. Hence, the underlying sheets are rather symmetric, which is why closure to vesicles seems reasonable. The favored closure to vesicular structures at lower surfactant contents is also in concordance with a study of Nieh et al. [15] and the obtained sizes from the CSPE model fit well with the diameter of the SUVs determined from the CMS fit (2000-3000 Å) which is another clear hint for the closure to SUV structures.

By model-dependent evaluation of exemplary SANS data of samples containing conventional DMPC as well as d54-DMPC with aescin contents x_{aescin} of 0, 10, 16 and 30 mol% we have shown that different structures are involved in the temperature-dependent structural phase behavior. Most of the structures adopted by the aescin-DMPC systems were representable by a sheet structure and therewith by the CSPE model. So far the samples were only investigated during the heating process. Therefore, the aim of the next subsection is to correlate the structural transition while cooling with the lipid's T_m.

3.3.4. *Proof of correlation of SUV/sheet-to-bicelle transition with the lipid's T_m*

Referring to the behavior observed in the turbidimetry experiment (Fig. 3), the sample containing 10 mol% aescin reconverts in a very narrow T_m-correlated one-step mechanism back to bicellar structures. SANS further showed that for this sample at $T > T_m$ extended sheets or SUVs structures are present. The reconversion process will now be followed by SANS and as well related to the T_m-values of the lipids which were determined before (compare Fig. S10). The SANS data for the sample containing 10 mol% aescin recorded during step-wise cooling from 27.5 to 10 °C for both, (a) DMPC and (b) d54-DMPC, are shown in Fig. 7.

As expressed by turbidimetry, also the step-wise recorded SANS data show a one-step reconversion back to small bicelles upon cooling. For both lipids, first hardly any changes in the scattering data can be observed upon cooling, even beyond the lipid's T_m (see T_m-related color encoding in Fig. 7). But, for both lipids again a clear shift in the reconversion temperature is detected. Hence, besides by turbidimetry the proposed correlation is proven by another independent method. Moreover, the correlation was even observable though two different approaches concerning the heating and cooling process were applied. Whereas in turbidimetry a continuous temperature profile was used, in SANS discrete steps of heating/cooling were used. Doing that, in addition we were able to prove that the correlation with the lipid's T_m is not a heating rate-dependent artifact (see also Fig. S6).

The scattering data were fitted with the CSPE model (blue and green lines in Fig. 7) and all fit parameters are summarized in Table S7. Similar as for a temperature of 35 °C in the heating cycle an extended lipid sheet with an approximate size of 1400x2000 Å^2 is still present in the cooling cycle. With decreasing T, the size of these sheets decreases slightly and the asymmetry increases. Interestingly, the decomposition into small, almost circular free standing bilayers with areas of ≈ 170x280 Å does not take place in a continuous process upon cooling. The A/D-ratio does not increase continuously in the sheet structures with decreasing T. Hence, the formation of bicelles does not take place in a step-wise process (no sequential splitting off of bicelle structures from the parent sheet structure). More likely, the reconversion seems to be hindered until a certain critical temperature is reached, at which the formation of bicelle structures is spontaneously possible again. The formation of an energetically *trapped state* is supported by NMR and a correlation with the lipid's T_m seems reasonable since 2D NOESY measurements stated that the bicelle formation in the DMPC-aescin system is controlled by interactions of DMPC and aescin within the hydrophobic membrane part [56].

A feature in the data for conventional DMPC also indicates formation of a *trapped state*. For the DMPC system a bump/peak in the scattering curve shows up at q ≈0.03 Å^{-1} for temperatures at which still sheet structures are present (down to 22.5 °C). For d54-DMPC, this feature is most probably not visible due to the head-tail contrast decreasing the scattering intensity in the mentioned q-range. The bump shifts to lower q-values with decreasing T (grey arrows in Fig. 7(a)), and a correlated membrane structure might be the reason for this bump [38]. Of course, a concrete structure at the molecular level cannot be proposed based on these data, but the following scenario seems possible: the decrease in T leads to a reduced solubility of the aescin molecules in the aqueous solution. It has previously been shown that the interaction of aescin with DMPC occurs mainly in the hydrophobic region of the membrane [56] and the interaction seems to be strongly enhanced if the membrane is present in the solid/crystalline phase. However, a directed interaction, which results in the formation of an aescin belt after penetration of aescin into the DMPC bilayer (and partly also demixing effects in the membrane), is only possible when the membrane entirely adopts the solid phase. This is only the case at a temperature significantly below T_m [63]. Therefore, it seems possible that the aescin molecules assemble on top/bottom of the large membrane fragments, which can lead to the formation of stacked membranes with 2-3 layers. When decreasing T, the continuous lipid membrane stiffens, leading to an increased membrane thickness and hence to a shift of the bump in the scattering data. After a significant part of the large membrane is present in the solid phase, penetration of the membrane by aescin molecules becomes possible, which leads to the abrupt formation of bicelles. In order to obtain a more accurate structural picture, further independent investigations would definitely have to be carried out.

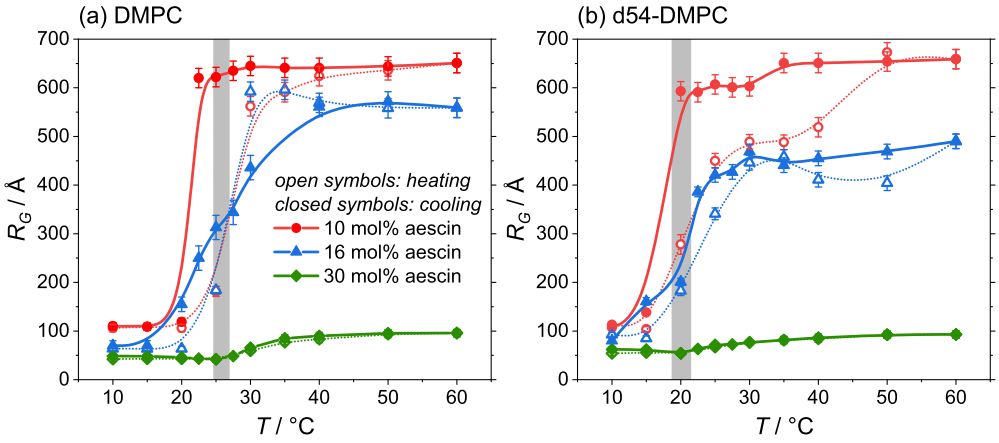

Fig. 8. Radius of gyration R_G derived from SANS data obtained via the IFT method for samples with different x_{aescin} prepared with (a) conventional DMPC and (b) chain-deuterated d54-DMPC. Corresponding approximations to the scattering curves are shown in Figs. S10-16. Grey vertical bars denote the corresponding phospholipid's T_m values (compare Fig. S9).

3.3.5. Model-independent evaluation: global size determination by IFT analysis - summary of temperature-dependent phase behavior

As seen previously, not all data can be adequately described by a single model, which means that a uniform parameter capable of characterizing the size of all found structures is absent. For this reason, an additional model-independent evaluation was carried out, which also included all measured SANS data and should provide a result analogous to the turbidimetry measurements. The model-independent Indirect Fourier Transformation (IFT) method was applied to derive the particle size in terms of the radius of gyration R_G. First, the $p(r)$-functions were determined from IFT (see Fig. S11-S17) and out of these the respective R_G was calculated (see Equation S4) [52,64]. The shape of the $p(r)$ functions nicely supports the results obtained from model-dependent fitting. The evaluation procedure as well as discussion of the $p(r)$-functions can be found in the Supplementary Material.

Fig. 8 shows the R_G values as a function of T while heating and subsequent cooling together with the T_m-values of both lipids (grey bars). A correlation of the size changes with T_m is also visible in this case. As mentioned before, contrary to the turbidimetry measurements, for the samples with 30 mol% aescin a size change becomes visible. For both lipids, bicelles with $R_{G,10\,°C} \approx$ 45-55 Å are present at low temperature, which enlarge at high temperature to $R_{G,60\,°C}$ values of ≈ 93-96 Å. In contrast to the samples with lower x_{aescin} a hysteresis effect is not found for the sample with 30 mol% aescin and the main size changes occur at $T > T_m$, independent of the lipid used. These structural changes will mostly originate from fast intra-particle rearrangements of the aescin molecules [56].

For the samples containing 10 and 16 mol% aescin, hysteresis can be observed, which is much more pronounced at the lower aescin content. As discussed already for the sample containing 10 mol% aescin for Fig. 7, the formation of solely bicelles is only possible if the lipid adapts a well-defined rigid phase. Due to the shift of the reconversion process to lower T for d54-DMPC, here again, the correlation of the structural reorganization with T_m is evidenced. For the sample containing 16 mol% aescin the two-step decomposition concluded from turbidimetry is indicated (compare Fig. 3). The step at lower temperature is only hardly visible due to the low number of data points in this T-region. This two-step reconversion again indicates that the behavior of the sample with 16 mol% lies in between the two extremes, namely the full conversion of bicelles to large sheets/vesicles at 10 mol% and the weak elongation of the bicelles at 30 mol% aescin.

3.4. Classification of the results of this study in the context of other publications

In this section, we would like to place the results of this study in a scientific context and compare them with previous publications. In general, the behavior of the system investigated here follows the accepted three-stage model [7–11]. The structures present under the conditions investigated are located in the middle of the phase diagram (second stage), which was proposed as a function of the detergent concentration under otherwise constant conditions (e.g. T = const.). Therefore, the DMPC membrane is saturated with aescin molecules and hence is dissolved into membrane fragments. This happens because $c_{aescin} > cmc_{aescin}$ applies and aescin itself tends to assemble at curved interfaces due to its packing parameter [10,12]. With increasing x_{aescin}, the size of the bicelle structures becomes smaller because more aescin molecules are available to cover the rim of the bicelles. With further increase of c_{aescin}, the DMPC-aescin aggregates would become more and more similar to pure aescin micelles.

Aescin itself forms micelles at $c_{aescin} > cmc_{aescin}$ and the structure of these micelles depends slightly on the temperature. At T = 10 °C (corresponding to $T < T_{m,DMPC}$) a rod-like structure is present, which changes into an elliptical shape at a temperature of T = 50 °C (corresponding to $T > T_{m,DMPC}$) [28]. In these rod-like structures, the aescin molecules form a large angle between each other. This is also the case in the bicelle structures, in which the aescin molecules are mainly found at the rim. The arrangement of the aescin molecules in the bicelles is therefore similar to that in the pure micellar structures. Incorporation into the continuous DMPC membrane cannot be ruled out but does not seem to be energetically preferred.

The structures described so far and the systematics depending on the detergent concentration can be found in many detergent-lipid systems [42,1,25,65]. As the temperature increases, the bicelle structures enlarge to form extended lipid sheets or even closed vesicles. This structural transformation is due to different factors: as the temperature increases, the solubility of the aescin in solution increases and aescin molecules are removed from the bicelle structures. In addition, the miscibility of the aescin molecules in the DMPC membrane increases, which is why some of the aescin molecules might migrate from the edge of the bicelle into the continuous DMPC bilayer [56]. Finally, the preference of aescin molecules to adopt an arrangement with a smaller bond angle at higher T could also have an influence on the structural rearrangement. Which type of aggregates (bicelles, extended sheets) are formed depends on the equilibrium of the miscibility of lipid and detergent and the lipids membrane rigidity [66,67]. Similarly, the closure of

large sheets into vesicles depends on the balance between bending rigidity and line tension [68]. In the case of the sample containing 10 mol% aescin, the line tension predominates over the bending rigidity, which leads to the formation of closed vesicles.

The formation of lipid sheets or vesicles upon T elevation was also observed for different detergent-lipid systems, such as a mixture of DMPC and the short-chain lipid 1,2-dihexanoyl-*sn*-glycero-3-phosphocholine (DHPC) [18,69] or octaethyleneglycol mono-n-dodecylether ($C_{12}E_8$) [43,44]. Similar observations were also made for a system of melittin, an amphipathic peptide, and the lipid 1,2-dihexadecanoyl-*sn*-glycero-3-phosphocholine (DPPC) [45] or DPPC and dihexanoyl-phosphatidylcholine, and dipalmitoyl-phosphatidylglycerol [70]. In all systems, structural changes occurred mainly in the range of T_m or were mostly completed above/below T_m of the lipid used. In the case of aescin, the interaction between detergent and lipid mainly takes place in the hydrophobic membrane region [56], which is why a dependence of the structure formation on T_m is not surprising. For the system of melittin and DMPC, as for the system investigated here, it was also found that the structural change is less pronounced the higher the concentration of detergent is [45].

In addition to the system investigated in this work, one other study focused on the reversibility of the structural transformation upon T-change. The amyloid-beta peptide (Aβ) was mixed with DMPC or DPPC and a transition from discoidal bicelle-like structures to SUVs was observed in multiple repetitions upon increasing/decreasing the temperature above T_m [71,46]. The largest change in the structure occurs in the range of T_m and no hysteresis effect is observed [46]. The reconversion of the vesicles to bicellular structures can be explained by the reversal of the effects mentioned above. Hence, the special feature of the study at hand is definitely the strong hysteresis effect that occurs for the sample with 10 mol% aescin. As already discussed above, this can probably be explained by an energetically trapped state in which different processes compete with each other: the reduced solubility of aescin in the aqueous solution due to T-reduction enforces an incorporation of aescin into the bicelles, but an ordered assembly of the aescin molecules at the edge of these structures is only spontaneously possible when large parts of the DMPC membrane have adopted the crystalline phase.

4. Conclusion

In this work, the significantly lowered $T_{m,d54\text{-}DMPC}$ value of chain-deuterated d54-DMPC (≈5 °C lower than $T_{m,DMPC}$) was used to relate the structural reorganization of DMPC-aescin mixtures with aescin contents between 10 and 30 mol% to the lipid's phase transition. To our knowledge, this is the first study exploiting the shifted T_m of a deuterated lipid for correlation with a T-dependent structural reorganization of a lipid-based system. First, the enlargement of the bicelle structures, present at $T < T_m$, was studied by dilution experiments and it was shown that a dilution of the samples to aescin concentrations below cmc_{aescin} leads to an increase of the size as well as the polydispersity of the aggregates, both caused by the removal of aescin molecules from the aggregates.

Temperature-dependent turbidimetry as well as SANS measurements showed that the overall behavior of the samples stays unaffected by the deuteration of the lipid and in all cases at temperatures well below T_m the formation of bicelles rim-stabilized by aescin molecules is confirmed. Upon heating to $T > T_m$ an extension of the bicelles in one preferred dimension was evidenced by model-dependent fitting. Whereas the enlargement of the bicelles is comparably small for very high aescin contents (30 mol%), significantly larger sheets are formed above T_m for intermediate aescin contents (16 mol%). The asymmetry of the sheets is lost for larger sheet sizes (and thus lower aescin content) with side lengths of ≈1000 Å. Hence, the closure of the sheets to vesicle structures is possible and is indeed proven by SANS measurements of DMPC- and d54-DMPC-based particles with an aescin content of 10 mol%.

The full reversibility of the reorganization processes was shown by performing consecutive heating-cooling cycles. A strong hysteresis was found in case of a low aescin content (especially 10 mol%), and therefore only in the case of the decomposition of extended sheets/vesicles upon temperature decrease. A complete conversion into large lipid sheets or closed vesicles at high temperature seems therefore to be the prerequisite for the observed hysteresis during cooling. The utilization of DMPC and d54-DMPC has proven the direct relation of the temperature-induced decomposition with the phospholipid's T_m. The final decrease of the temperature well below T_m seems to facilitate a strong interaction of DMPC and aescin, resulting in the recovery of bicelles. Since the decomposition occurs in a steep one-step process formation of a trapped state, originating from the interactions of aescin and DMPC in the hydrophobic membrane region, seems likely. Contrary, the sample with the highest aescin content (30 mol%) showed only a small enlargement of the bicelles upon temperature increase and moreover no indication of hysteresis. For mid aescin concentrations, a combination of both extremes - the closure to vesicles and the weakly pronounced elongation in a preferred dimension - was observed, indicating that the whole structural conversion related to an increasing aescin content is continuous. The interactions between a lipid and a detergent, e.g. a saponin, are complex and, to our knowledge, such strong hysteresis effects, especially accompanied by the formation of a trapped state have not been reported before.

CRediT authorship contribution statement

Carina Dargel: Writing – review & editing, Writing – original draft, Visualization, Validation, Project administration, Methodology, Investigation, Formal analysis, Data curation, Conceptualization. **Lara H. Moleiro:** Writing – review & editing, Investigation. **Aurel Radulescu:** Writing – review & editing, Methodology, Investigation. **Tim Julian Stank:** Data curation, Investigation, Writing – review & editing. **Thomas Hellweg:** Writing – review & editing, Validation, Supervision, Project administration, Funding acquisition.

Declaration of competing interest

The authors declare that they have no known competing financial interests or personal relationships that could have appeared to influence the work reported in this paper.

Acknowledgement

Financial support by the Deutsche Forschungsgemeinschaft (DFG) (HE2995/7-1, INST 215/432-1 FUGG) is gratefully acknowledged. The authors thank the JCNS at Heinz-Maier-Leibnitz Zentrum (MLZ), Garching, Germany for allocation of beamtime at the KWS-2 beamline (proposal number: 12673).

This work benefited from the use of the SasView application, originally developed under NSF award DMR-0520547. SasView contains code developed with funding from the European Union's Horizon 2020 research and innovation program under the SINE2020 project, grant agreement No 654000.

Appendix A. Supplementary Material

Supplementary Material related to this article can be found online at https://doi.org/10.1016/j.jcis.2024.10.074.

Data availability

Data will be made available on request.

References

[1] U.H. Dürr, R. Soong, A. Ramamoorthy, When detergent meets bilayer: birth and coming of age of lipid bicelles, Prog. Nucl. Magn. Reson. Spectrosc. 69 (2013) 1.

[2] J. Katsaras, T.A. Harroun, J. Pencer, M.-P. Nieh, "Bicellar" lipid mixtures as used in biochemical and biophysical studies, Naturwissenschaften 92 (8) (2005) 355–366.
[3] W. Zhang, J. Sun, Z. He, The application of open disk-like structures as model membrane and drug carriers, Asian J. Pharm. Sci. 8 (3) (2013) 143–150.
[4] M. Jamshad, Y.-P. Lin, T.J. Knowles, R.A. Parslow, C. Harris, M. Wheatley, D.R. Poyner, R.M. Bill, O.R.T. Thomas, M. Overduin, T.R. Dafforn, Surfactant-free purification of membrane proteins with intact native membrane environment, Biochem. Soc. Trans. 39 (3) (2011) 813–818.
[5] C.R. Sanders, R.S. Prosser, Bicelles: a model membrane system for all seasons?, Structure 6 (10) (1998) 1227–1234.
[6] C.R. Sanders, G.C. Landis, Reconstitution of membrane proteins into lipid-rich bilayered mixed micelles for NMR studies, Biochemistry 34 (12) (1995) 4030–4040.
[7] D. Lichtenberg, R.J. Robson, E.A. Dennis, Solubilization of phospholipids by detergents structural and kinetic aspects, Bioch. Biophys. Acta, Rev. Biomembr. 737 (2) (1983) 285–304.
[8] A. Hildebrand, R. Neubert, P. Garidel, A. Blume, Bile salt induced solubilization of synthetic phosphatidylcholine vesicles studied by isothermal titration calorimetry, Langmuir 18 (7) (2002) 2836–2847.
[9] N.A. Mazer, G.B. Benedek, M.C. Carey, Quasielastic light-scattering studies of aqueous biliary lipid systems. Mixed micelle formation in bile salt-lecithin solutions, Biochemistry 19 (4) (1980) 601–615.
[10] D. Lichtenberg, E. Opatowski, M.M. Kozlov, Phase boundaries in mixtures of membrane-forming amphiphiles and micelle-forming amphiphiles, Biochim. Biophys. Acta, Biomembr. 1508 (1–2) (2000) 1–19.
[11] A. Helenius, K. Simons, Solubilization of membranes by detergents, Biochim. Biophys. Acta, Rev. Biomembr. 415 (1) (1975) 29–79.
[12] J.N. Israelachvili, Intermolecular and Surface Forces, Academic Press, 2015.
[13] J.S. Pedersen, S.U. Egelhaaf, P. Schurtenberger, Formation of polymerlike mixed micelles and vesicles in lecithin-bile salt solutions: a small-angle neutron-scattering study, J. Phys. Chem. 99 (4) (1995) 1299–1305.
[14] P. Lesieur, M. Kiselev, L. Barsukov, D. Lombardo, Temperature-induced micelle to vesicle transition: kinetic effects in the DMPC/NaC system, J. Appl. Crystallogr. 33 (3–1) (2000) 623–627.
[15] M.-P. Nieh, C.J. Glinka, S. Krueger, R.S. Prosser, J. Katsaras, SANS study on the effect of lanthanide ions and charged lipids on the morphology of phospholipid mixtures, Biophys. J. 82 (5) (2002) 2487–2498.
[16] M.-P. Nieh, V.A. Raghunathan, S.R. Kline, T.A. Harroun, C.-Y. Huang, J. Pencer, J. Katsaras, Spontaneously formed unilamellar vesicles with path-dependent size distribution, Langmuir 21 (15) (2005) 6656–6661.
[17] V.A. Bjørnestad, R. Lund, Pathways of membrane solubilization: a structural study of model lipid vesicles exposed to classical detergents, Langmuir 39 (11) (2023) 3914–3933.
[18] S. Mahabir, D. Small, M. Li, W. Wan, N. Kučerka, K. Littrell, J. Katsaras, M.-P. Nieh, Growth kinetics of lipid-based nanodiscs to unilamellar vesicles—a time-resolved small angle neutron scattering (SANS) study, Biochim. Biophys. Acta, Biomembr. 1828 (3) (2013) 1025–1035.
[19] A. Walter, P.K. Vinson, A. Kaplun, Y. Talmon, Intermediate structures in the cholate-phosphatidylcholine vesicle-micelle transition, Biophys. J. 60 (6) (1991) 1315–1325, https://doi.org/10.1016/S0006-3495(91)82169-5.
[20] M.A. Long, E.W. Kaler, S.P. Lee, Structural characterization of the micelle-vesicle transition in lecithin-bile salt solutions, Biophys. J. 67 (4) (1994) 1733–1742.
[21] P. Schurtenberger, N. Mazer, W. Känzig, Micelle to vesicle transition in aqueous solutions of bile salt and lecithin, J. Phys. Chem. 89 (6) (1985) 1042–1049.
[22] M.A. Kiselev, D. Lombardo, Structural characterization in mixed lipid membrane systems by neutron and X-ray scattering, Biochim. Biophys. Acta G, Gen. Subj. 1861 (1) (2017) 3700–3717.
[23] M. Kiselev, M. Janich, A. Hildebrand, P. Strunz, R. Neubert, D. Lombardo, Structural transition in aqueous lipid/bile salt [DPPC/NaDC] supramolecular aggregates: SANS and DLS study, Chem. Phys. 424 (2013) 93–99.
[24] L. Jiang, K. Wang, M. Deng, Y. Wang, J. Huang, Bile salt-induced vesicle-to-micelle transition in catanionic surfactant systems: steric and electrostatic interactions, Langmuir 24 (9) (2008) 4600–4606.
[25] M. Li, H.H. Morales, J. Katsaras, N. Kučerka, Y. Yang, P.M. Macdonald, M.-P. Nieh, Morphological characterization of DMPC/CHAPSO bicellar mixtures: a combined SANS and NMR study, Langmuir 29 (51) (2013) 15943–15957.
[26] Ö. Güçlü-Üstündağ, G. Mazza, Saponins: properties, applications and processing, Crit. Rev. Food Sci. Nutr. 47 (3) (2007) 231–258.
[27] G. Francis, Z. Kerem, H.P. Makkar, K. Becker, The biological action of saponins in animal systems: a review, Br. J. Nutr. 88 (6) (2002) 587–605.
[28] C. Dargel, R. Geisler, Y. Hannappel, I. Kemker, N. Sewald, T. Hellweg, Self-assembly of the bio-surfactant aescin in solution: a small-angle X-ray scattering and fluorescence study, Colloids Interfaces 3 (2) (2019) 47, https://doi.org/10.3390/colloids3020047.
[29] R. Sreij, C. Dargel, L.H. Moleiro, F. Monroy, T. Hellweg, Aescin incorporation and nanodomain formation in DMPC model membranes, Langmuir 33 (43) (2017) 12351–12361.
[30] M. Dudek-Makuch, E. Studzińska-Sroka, Horse chestnut–efficacy and safety in chronic venous insufficiency: an overview, Rev. Bras. Farmacog. 25 (5) (2015) 533–541.
[31] J.A. Wilkinson, A.M.G. Brown, Horse chestnut aesculus hippocastanum: potential applications in cosmetic skin-care products, Int. J. Cosmet. Sci. 21 (6) (1999) 437–447.
[32] C.R. Sirtori, Aescin: pharmacology, pharmacokinetics and therapeutic profile, Pharmacol. Res. 44 (3) (2001) 183–193.
[33] T. Hellweg, T. Sottmann, J. Oberdisse, Recent advances in biosurfactant-based association colloids—self-assembly in water, Front. Soft Matter 2 (2023) 1081877.
[34] K. Wojciechowski, I. Jurek, I. Góral, M. Campana, T. Geue, T. Gutberlet, Surface-active extracts from plants rich in saponins–effect on lipid mono- and bilayers, Surf. Interfaces 27 (2021) 101486.
[35] S. Böttger, K. Hofmann, M.F. Melzig, Saponins can perturb biologic membranes and reduce the surface tension of aqueous solutions: a correlation?, Bioorg. Med. Chem. 20 (9) (2012) 2822–2828.
[36] R. Geisler, C. Dargel, T. Hellweg, The biosurfactant β-aescin: a review on the physicochemical properties and its interaction with lipid model membranes and Langmuir monolayers, Molecules 25 (1) (2019) 117.
[37] R. Sreij, C. Dargel, P. Geisler, Y. Hertle, A. Radulescu, S. Pasini, J. Perez, L.H. Moleiro, T. Hellweg, DMPC vesicle structure and dynamics in the presence of low amounts of the saponin aescin, Phys. Chem. Chem. Phys. 20 (14) (2018) 9070–9083.
[38] R. Sreij, C. Dargel, Y. Hannappel, J. Jestin, S. Prévost, R. Dattani, O. Wrede, T. Hellweg, Temperature dependent self-organization of DMPC membranes promoted by intermediate amounts of the saponin aescin, Biochim. Biophys. Acta, Biomembr. 1861 (5) (2019) 897–906.
[39] R. Geisler, M.C. Pedersen, Y. Hannappel, R. Schweins, S. Prévost, R. Dattani, L. Arleth, T. Hellweg, Aescin-induced conversion of gel-phase lipid membranes into bicelle-like lipid nanoparticles, Langmuir 35 (49) (2019) 16244–16255.
[40] R. Geisler, M.C. Pedersen, N. Preisig, Y. Hannappel, S. Prévost, R. Dattani, L. Arleth, T. Hellweg, Aescin–a natural soap for the formation of lipid nanodiscs with tunable size, Soft Matter 17 (7) (2021) 1888–1900.
[41] L.H. Moleiro, M.T. Martín-Romero, D. Herráez-Aguilar, J.A. Santiago, N. Caselli, C. Dargel, R. Geisler, T. Hellweg, F. Monroy, Dual mechanical impact of β-escin on model lipid membranes, Front. Soft Matter 3 (2023) 1240878.
[42] C. Dargel, Y. Hannappel, T. Hellweg, Heating-induced DMPC/glycyrrhizin bicelle-to-vesicle transition: a X-ray contrast variation study, Biophys. J. 118 (10) (2020) 2411–2425.
[43] D. Otten, L. Löbbecke, K. Beyer, Stages of the bilayer-micelle transition in the system phosphatidylcholine-C12E8 as studied by deuterium- and phosphorous-NMR, light scattering, and calorimetry, Biophys. J. 68 (2) (1995) 584–597.
[44] S.S. Funari, B. Nuscher, G. Rapp, K. Beyer, Detergent-phospholipid mixed micelles with a crystalline phospholipid core, Proc. Natl. Acad. Sci. 98 (16) (2001) 8938–8943.
[45] E.J. Dufourc, J.-F. Faucon, G. Fourche, J. Dufourcq, T. Gulik-Krzywicki, M. le Maire, Reversible disc-to-vesicle transition of melittin-DPPC complexes triggered by the phospholipid acyl chain melting, FEBS Lett. 201 (2) (1986) 205–209.
[46] O. Ivankov, T.N. Murugova, E.V. Ermakova, T. Kondela, D.R. Badreeva, P. Hrubovčák, D. Soloviov, A. Tsarenko, A. Rogachev, A.I. Kuklin, et al., Amyloid-beta peptide (25–35) triggers a reorganization of lipid membranes driven by temperature changes, Sci. Rep. 11 (1) (2021) 21990.
[47] K.A. Rubinson, Practical corrections for p(H,D) measurements in mixed H_2O/D_2O biological buffers, Anal. Methods 9 (2017) 2744–2750, https://doi.org/10.1039/C7AY00669A.
[48] S.W. Provencher, CONTIN: a general purpose constrained regularization program for inverting noisy linear algebraic and integral equations, Comput. Phys. Commun. 27 (3) (1982) 229–242.
[49] T. Kourti, Turbidimetry in Particle Size Analysis, Encyclopedia of Analytical Chemistry: Applications, Theory and Instrumentation, vol. 4, Wiley, Chichester, 2000, p. 344.
[50] O. Glatter, A new method for the evaluation of small-angle scattering data, J. Appl. Crystallogr. 10 (5) (1977) 415–421.
[51] D.I. Svergun, M.H. Koch, Small-angle scattering studies of biological macromolecules in solution, Rep. Prog. Phys. 66 (10) (2003) 1735.
[52] A. Bergmann, G. Fritz, O. Glatter, Solving the generalized indirect Fourier transformation (GIFT) by Boltzmann simplex simulated annealing (BSSA), J. Appl. Crystallogr. 33 (5) (2000) 1212–1216.
[53] SASView, Freeware version 4.2.0, http://www.sasview.org, 2018.
[54] A. Radulescu, V. Pipich, H. Frielinghaus, M.-S. Appavou, KWS-2, the high intensity/wide Q-range small-angle neutron diffractometer for soft-matter and biology at FRM II, J. Phys. Conf. Ser. 351 (1) (2012) 012026.
[55] V. Pipich, QtiKWS: user-friendly program for reduction, visualization, analysis and fit of SA(N)S data, http://www.qtikws.de, 2012, http://www.qtikws.de.
[56] F. Escobedo, M. Gospalswamy, P. Hägerbäumer, T.J. Stank, J. Victor, G. Groth, H. Gohlke, C. Dargel, T. Hellweg, M. Etzkorn, Characterization of size-tuneable aescin-lipid nanoparticles as platform for stabilization of membrane proteins, Colloids Surf. B, Biointerfaces 242 (2024) 114071, https://doi.org/10.1016/j.colsurfb.2024.114071.
[57] C. Dargel, F. Gräbitz-Bräuer, R. Geisler, P. Fandrich, Y. Hannappel, L. Porcar, T. Hellweg, Stable DOPG/glycyrrhizin vesicles with a wide range of mixing ratios: structure and stability as seen by scattering experiments and cryo-TEM, Molecules 26 (16) (2021) 4959.
[58] F. Gräbitz-Bräuer, C. Dargel, R. Geisler, P. Fandrich, V. Sabadasch, L. Porcar, A. Mix, T. Hellweg, Coexistence of DOPG model membranes and β-aescin micelles: a combined scattering and NMR study, Colloid Polym. Sci. (2023) 1–14.

[59] J. Penfold, R.K. Thomas, I. Tucker, J.T. Petkov, S.D. Stoyanov, N. Denkov, K. Golemanov, S. Tcholakova, J.R.P. Webster, Saponin adsorption at the air-water interface: neutron reflectivity and surface tension study, Langmuir 34 (32) (2018) 9540–9547.
[60] D. Singh, Small Angle Scattering Studies of Self Assembly in Lipid Mixtures, The Johns Hopkins University, 2008, PhD thesis.
[61] M.-P. Nieh, N. Kučerka, J. Katsaras, Formation mechanism of self-assembled unilamellar vesicles, Can. J. Phys. 88 (10) (2010) 735–740.
[62] C.-P. Chng, Effect of simulation temperature on phospholipid bilayer–vesicle transition studied by coarse-grained molecular dynamics simulations, Soft Matter 9 (30) (2013) 7294–7301.
[63] T. Heimburg, A model for the lipid pretransition: coupling of ripple formation with the chain-melting transition, Biophys. J. 78 (3) (2000) 1154–1165.
[64] O. Glatter, G. Fritz, H. Lindner, J. Brunner-Popela, R. Mittelbach, R. Strey, S.U. Egelhaaf, Nonionic micelles near the critical point: micellar growth and attractive interaction, Langmuir 16 (23) (2000) 8692–8701.
[65] S.D. McCalpin, T. Ravula, A. Ramamoorthy, Saponins form nonionic lipid nanodiscs for protein structural studies by nuclear magnetic resonance spectroscopy, J. Phys. Chem. Lett. 13 (7) (2022) 1705–1712.
[66] V.A. Bjørnestad, R. Lund, Pathways of membrane solubilization: a structural study of model lipid vesicles exposed to classical detergents, Langmuir 39 (11) (2023) 3914–3933.
[67] E. Johansson, M.C. Sandström, M. Bergström, K. Edwards, On the formation of discoidal versus threadlike micelles in dilute aqueous surfactant/lipid systems, Langmuir 24 (5) (2008) 1731–1739.
[68] K. Bressel, M. Muthig, S. Prévost, I. Grillo, M. Gradzielski, Mesodynamics: watching vesicle formation in situ by small-angle neutron scattering, Colloid Polym. Sci. 288 (2010) 827–840.
[69] A. Flynn, M. Ducey, A. Yethiraj, M.R. Morrow, Dynamic properties of bicellar lipid mixtures observed by rheometry and quadrupole echo decay, Langmuir 28 (5) (2012) 2782–2790.
[70] I. Alahmadi, D. Hoy Jr, A. Tahmasbi Rad, S. Patil, A. Alahmadi, J. Kinnun, H.L. Scott, J. Katsaras, M.-P. Nieh, Changes experienced by low-concentration lipid bicelles as a function of temperature, Langmuir 38 (14) (2022) 4332–4340.
[71] S. Kurakin, D. Badreeva, E. Dushanov, A. Shutikov, S. Efimov, A. Timerova, T. Mukhametzyanov, T. Murugova, O. Ivankov, K. Mamatkulov, et al., Arrangement of lipid vesicles and bicelle-like structures formed in the presence of Aβ (25–35) peptide, Biochim. Biophys. Acta, Biomembr. 1866 (1) (2024) 184237.